# Coronagraphic Reconstruction of the Open-Field Solar Corona Using QRaFT Technique

V. Uritsky[1,2], C. Rura[1,2], S. Jones[1,2], C. Downs[3], N. Arge[1], N. Alzate[1,4], and M. Casti[1,2]

1) Catholic University of America
2) NASA GSFC
3) Predictive Science Inc
4) ADNET Systems

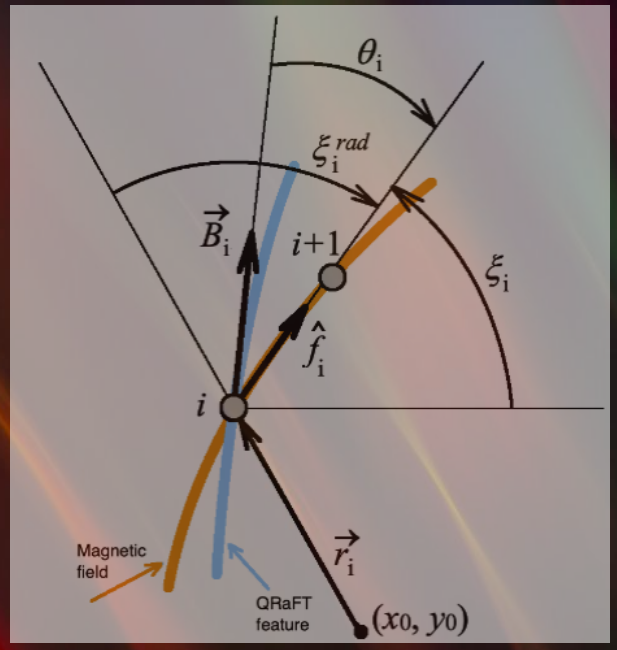

# Talk outline

- The role of ambient SW in space weather forecasting
- Coronal magnetic field from image segmentation
- The Quasi-Radial Field Line Tracing (QRaFT) methodology
- Validating QRaFT using synthetic and real-life coronal data
- Conclusions and future work

# Background SW conditions are critical for space weather

A CME on Dec 02 2003

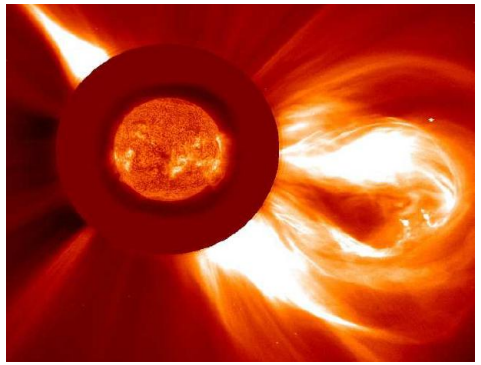

SOHO LASCO C2

B

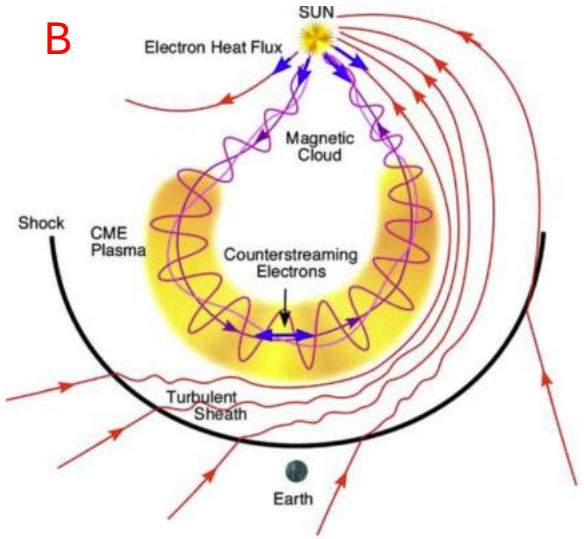


Zurbuchen & Richardson, Space Sci Ser ISSI 2006

C Simulated disturbance (WAS-ENLIL-Cone)

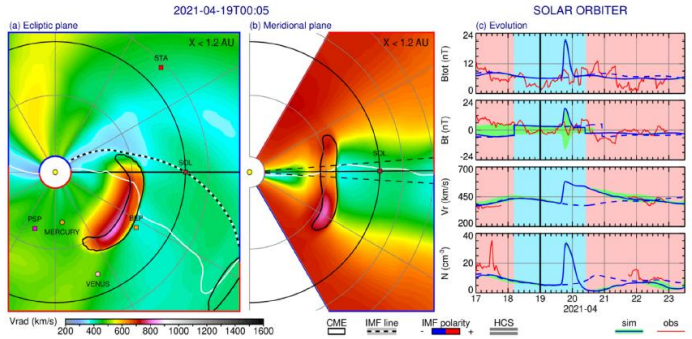


Multi-CMEs in late March 2022

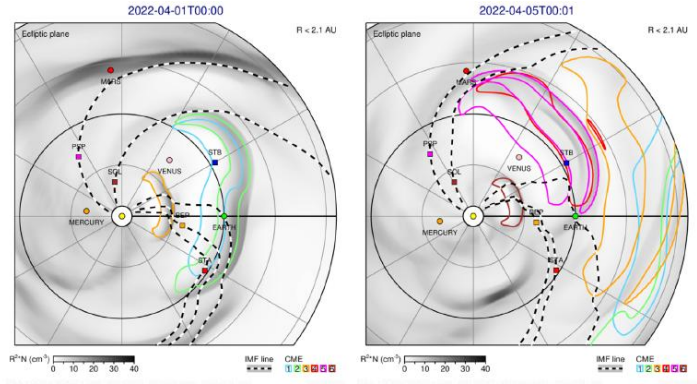


TABLE 2 Geometric and kinematic parameters of CMEs in late-March 2022 (from DONKI catalog for ENLIL simulation with results shown in Figures 3, 5).

| CME | Leading edge at 21.5 Rs | Latitude (deg) | Longitude (deg) | Rmajor (deg) | Speed (km/s) | DONKI M2M catalog ID |
|---|---|---|---|---|---|---|
| 1 | 2022-03-28T17:19 | 7 | 12 | 45 | 662 | 2022-03-28T12:09:00-CME-001 |
| 2 | 2022-03-29T00:58 | 3 | 3 | 50 | 760 | 2022-03-28T20:23:00-CME-001 |
| 3 | 2022-03-30T21:49 | 0 | 15 | 40 | 808 | 2022-03-30T18:23:00-CME-001 |
| 4 | 2022-04-01T00:54 | −3 | 48 | 35 | 576 | 2022-03-31T19:09:00-CME-001 |
| 5 | 2022-04-02T16:12 | −15 | 54 | 45 | 1,370 | 2022-04-02T13:38:00-CME-001 |
| 6 | 2022-04-03T21:19 | −4 | 22 | 35 | 702 | 2022-04-03T16:38:00-CME-001 |

D. Odstrcil, Front. Astron. &Space Sci 2023

D

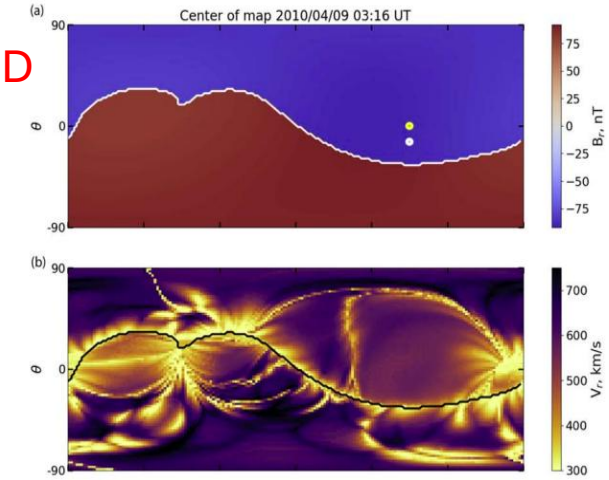


Background SW boundary conditions from WSA-ADAPT used in GAMERA simulation

CME magnetic field at t=19hr, r=21.5Rs (CR2095)

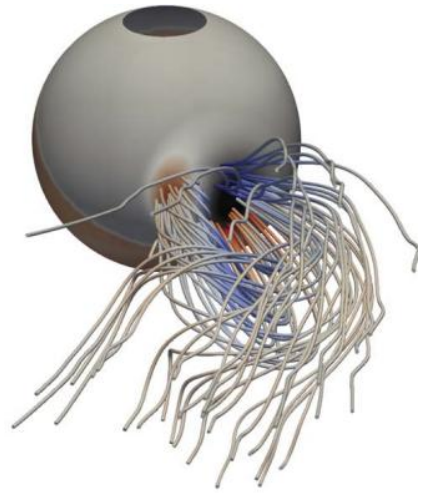

E. Provornikova et al., ApJ 2024

**PUNCH images may revolutionize our understanding of the *background* SW / IMF**

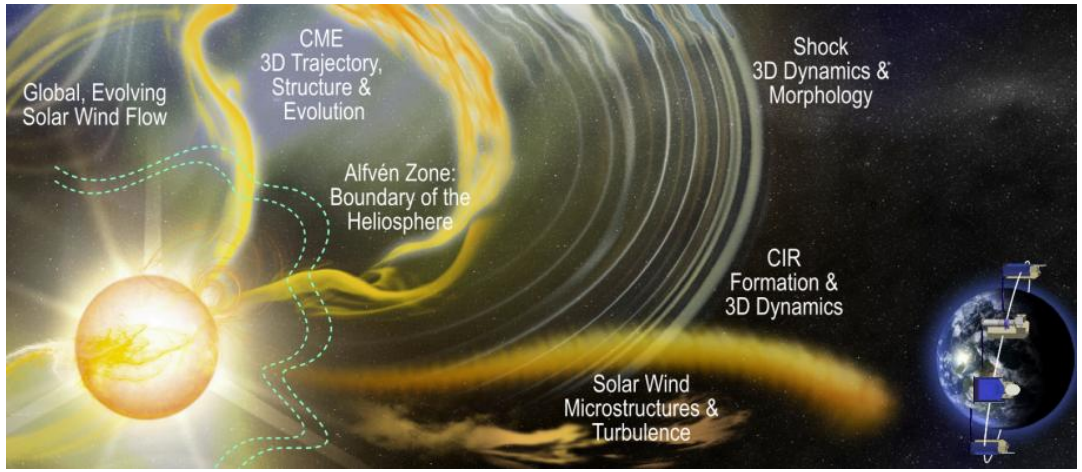

# Segmenting coronal images

## Closed field / active regions

A

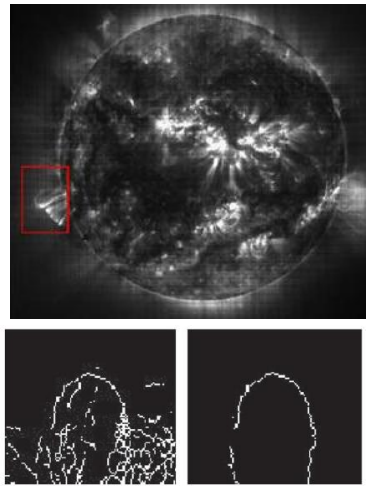

N. Durak et al., Pattern Recognition 2009

B

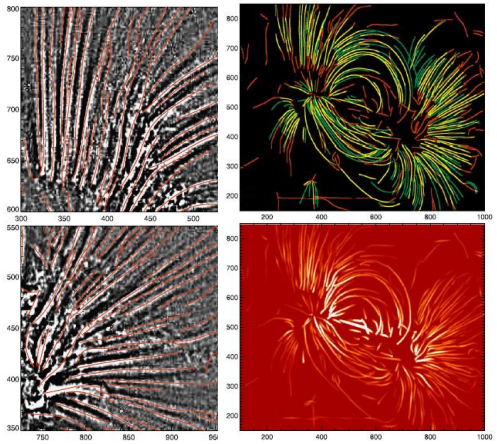

M. Aschwanden, Sol. Phys 2010; Entropy 2014

C

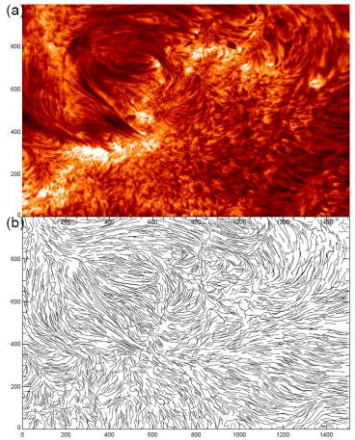

D

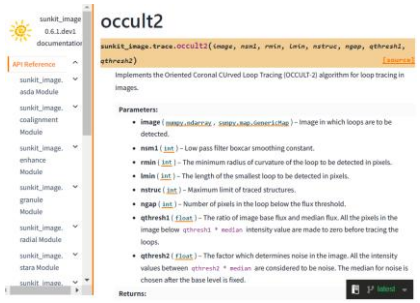


sunpy / UCCULT2

E

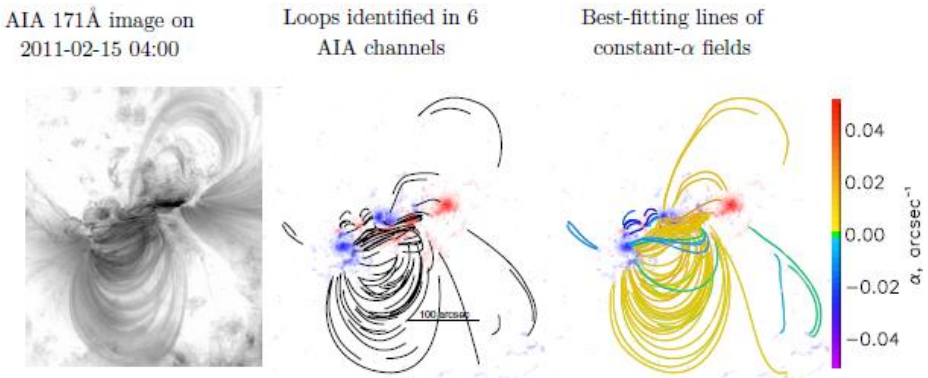


A. Malanushenko et al., ApJ 2014

## Open field / TSE

F

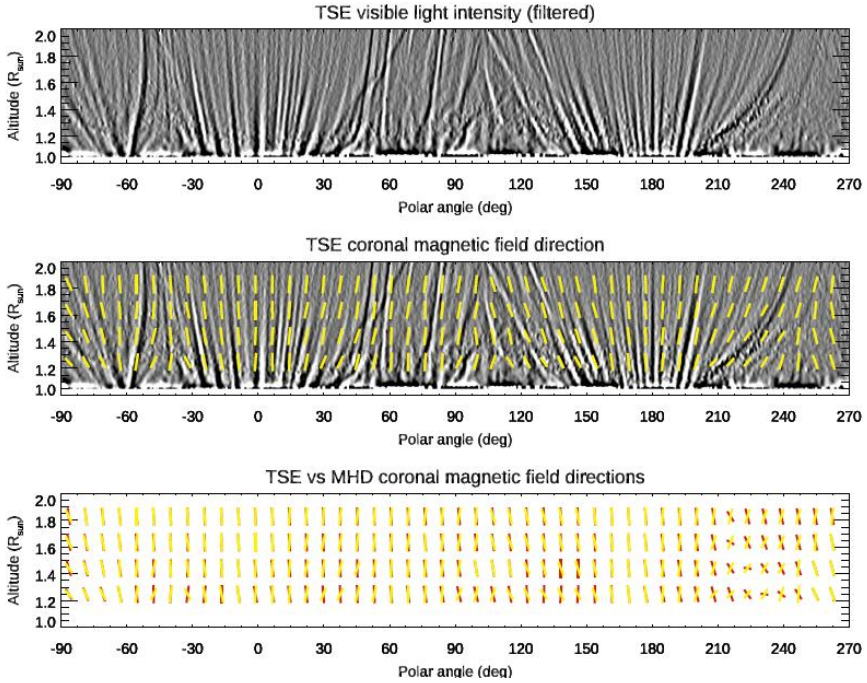


A. Bemporad, ApJ 2020, 2023

G

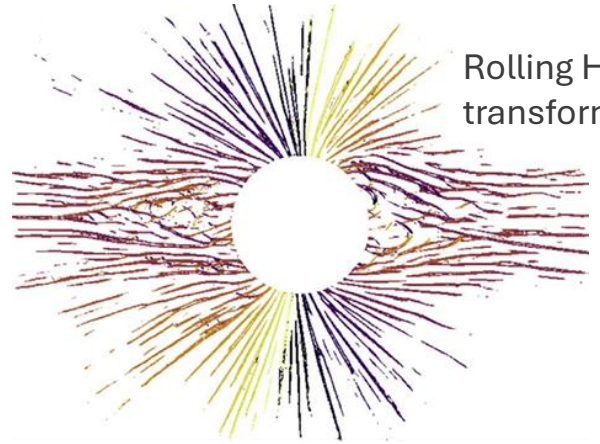

Rolling Hough transform (RHT)

B. Boe, Habbal & Druckmüller, ApJ 2020

# The Quasi-Radial Field Line Tracing (QRaFT) methodology

A

MLSO K-Kor / 2016 May 27

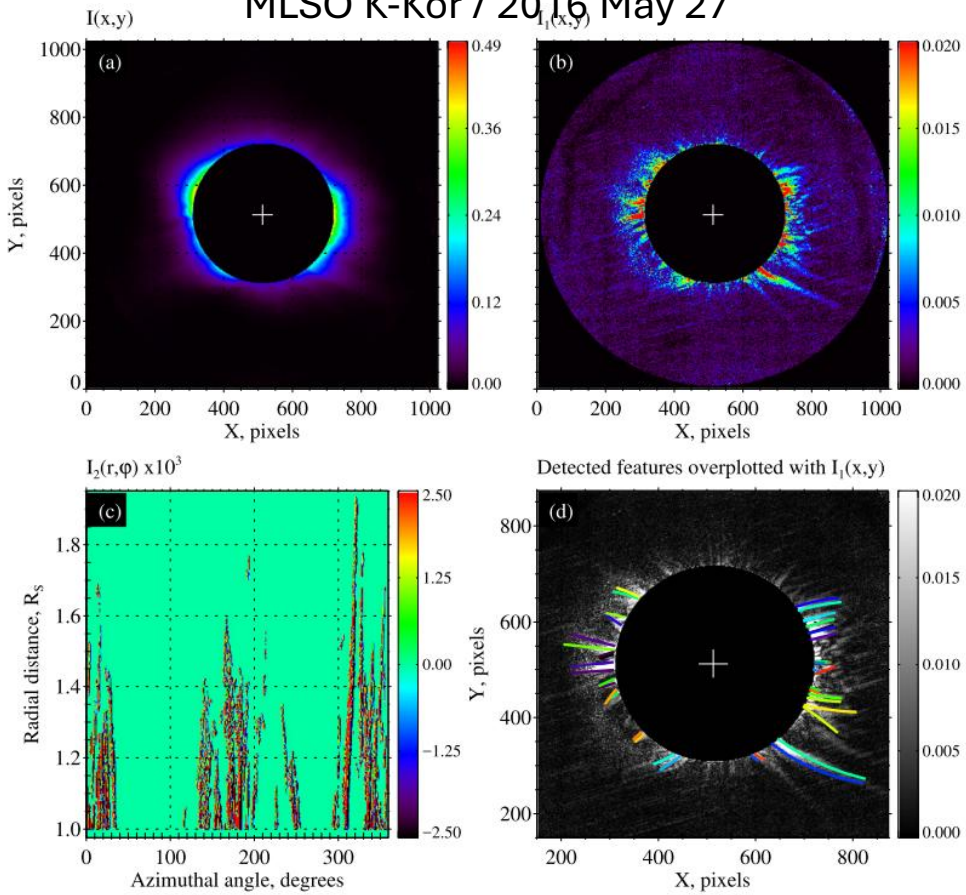


V. Uritsky, GitHub / Zenode 2022, 10.5281/zenodo.7410948

github.com/uritsky/QRaFT

The Astrophysical Journal, 896:57 (9pp), 2020 June 10 https://doi.org/10.3847/1538-4357/ab8cb9


## Improving Coronal Magnetic Field Models Using Image Optimization

Shaela I. Jones[1,2], Vadim M. Uritsky[1,2], Joseph M. Davila[1], and Vladimir N. Troyan[3]
[1] NASA Goddard Space Flight Center, Code 670, Greenbelt, MD 20771, USA; shaela.i.jonesmecholsky@nasa.gov
[2] Catholic University of America, USA
[3] Saint Petersburg State University, Russia
*Received 2019 March 7; revised 2020 April 20; accepted 2020 April 22; published 2020 June 12*

B

$$J = \beta \sum_{k=1}^{N} |\theta_{o,k} - \theta_{m,k}|^2 + \gamma\, O$$

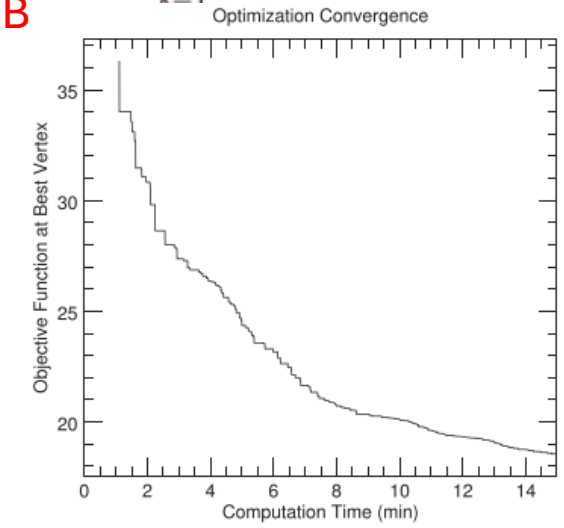


C

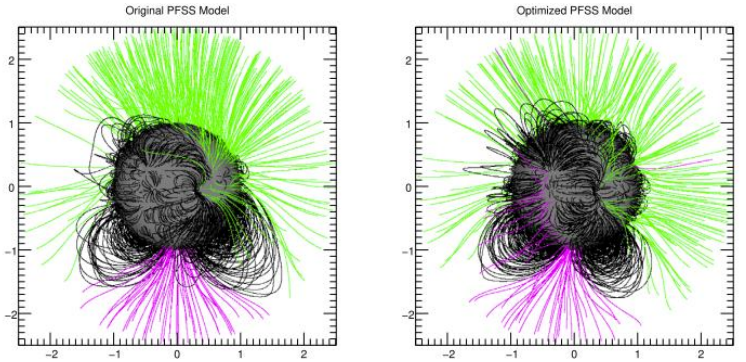


D

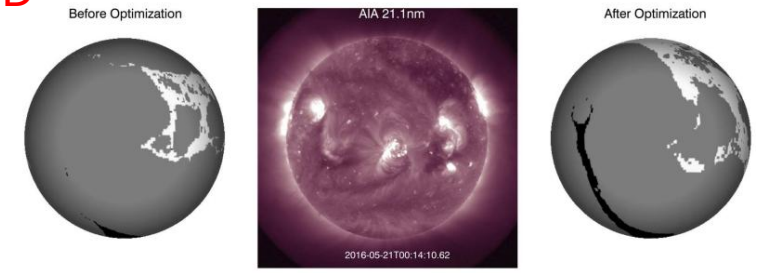


S. Jones et al., ApJ 2016, 2017, 2020

# QRaFT 3.0 data processing pipeline

## Image enhancement

### Radial detrending

$$I_{tr}(r) = \langle I(x,y) \rangle_{\Omega(r)},$$

$$\Omega(r) = \{(x,y) \,|\, (x-x_0)^2 + (y-y_0)^2 = r^2\}$$

$$I_{detr}(x,y) = I(x,y) - I_{tr}\left(\sqrt{(x-x_0)^2 + (y-y_0)^2}\right)$$

### Coordinate transformation

$$I_{detr}(x,y) \rightarrow I(\phi,\rho)$$

### Anisotropic smoothing

$$I_s(\phi,\rho) = \frac{1}{\Delta\phi_s \Delta\rho_s} \int_{\rho-\Delta\rho_s/2}^{\rho+\Delta\rho_s/2} \int_{\phi-\Delta\phi_s/2}^{\phi+\Delta\phi_s/2} I(\phi',\rho')\, d\phi'\, d\rho'$$

### Azimuthal differencing

$$I''(\phi,\rho) = |I_s(\phi-\Delta\phi/2,\rho) + I_s(\phi+\Delta\phi/2,\rho) - 2I_s(\phi,\rho)|$$

### Azimuthal detrending

$$I''_{tr}(\phi) = \frac{1}{\Delta\phi_d} \int_{\phi-\Delta\phi_d/2}^{\phi+\Delta\phi_d/2} \langle I''_s(\phi',\rho) \rangle_\rho \, d\phi'$$

$$I_{enh}(\phi,\rho) = \frac{I''(\phi,\rho)}{I''_{tr}(\phi)}$$

## Feature tracing

### Adaptive thresholding

$$\frac{\sum_{\phi,\rho} \mathcal{H}\left(I_{enh}(\phi,\rho) - I_k^{th}\right)}{N} = p_k$$

### Blob detection

$$I_{enh}(\phi, \rho > \rho_j^{\min}) > I_k^{th} \;\rightarrow\; \Lambda_{j,k}(\phi,\rho) \in \{1, \ldots, \lambda_{j,k}^{\max}\}$$

### Feature coordinates

$$\Phi_\lambda(\rho) = \{\phi \,|\, \Lambda(\phi,\rho) = \lambda\}$$

$$R_\lambda = \{\rho \,|\, (\exists\phi)[\Lambda(\phi,\rho) = \lambda]\}$$

$$\rho_{\lambda,i} = \min R_\lambda + i \times \Delta\rho$$

$$\phi_{\lambda,i} = \langle \Phi_\lambda(\rho_{\lambda,i}) \rangle$$

### Polynomial interpolation

$$\phi^*_{\lambda,i} = \sum_{m=0}^{M} a_{\lambda,m}\, \rho^m_{\lambda,i}$$

B

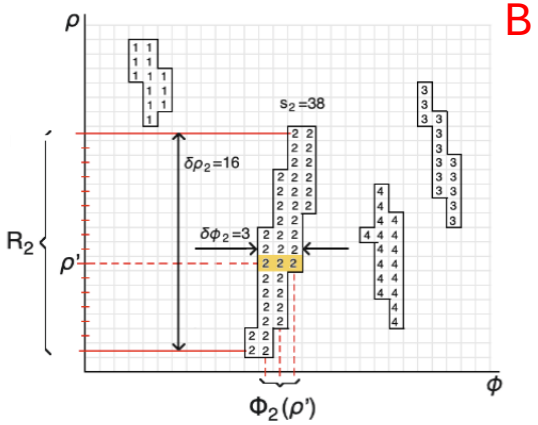


## Feature metrics

### Feature dimensions

$$\delta\phi_\lambda = \max_\rho |\Phi_\lambda(\rho)|$$

$$\delta\rho_\lambda = \max R_\lambda - \min R_\lambda$$

$$s_\lambda = |\{(\phi,\rho) \,|\, \Lambda(\phi,\rho) = \lambda\}|$$

### POS positions

$$x_{\lambda,i} = \rho_{\lambda,i} \cos\phi^*_{\lambda,i} + x_0$$

$$y_{\lambda,i} = \rho_{\lambda,i} \sin\phi^*_{\lambda,i} + y_0$$

### POS orientation angles

$$\xi_{\lambda,i} = \tan^{-1}\left(\frac{y_{\lambda,i+1} - y_{\lambda,i}}{x_{\lambda,i+1} - x_{\lambda,i}}\right)$$

$$\xi^{rad}_{\lambda,i} = \tan^{-1}\left(\frac{y_{\lambda,i} - y_0}{x_{\lambda,i} - x_0}\right)$$

### Misalignment angles

$$h_{\lambda,i} = 2\mathcal{H}(\vec{B}_{\lambda,i} \cdot \vec{r}_{\lambda,i}) - 2 = \begin{cases} +1, & \vec{B}_{\lambda,i} \text{ is outward} \\ -1, & \vec{B}_{\lambda,i} \text{ is inward} \end{cases}$$

$$\theta_{\lambda,i} = \sin^{-1}\left(\frac{\hat{f}_{\lambda,i} \times (h_{\lambda,i}\, \vec{B}_{\lambda,i})}{|\vec{B}_{\lambda,i}|}\right)$$

A

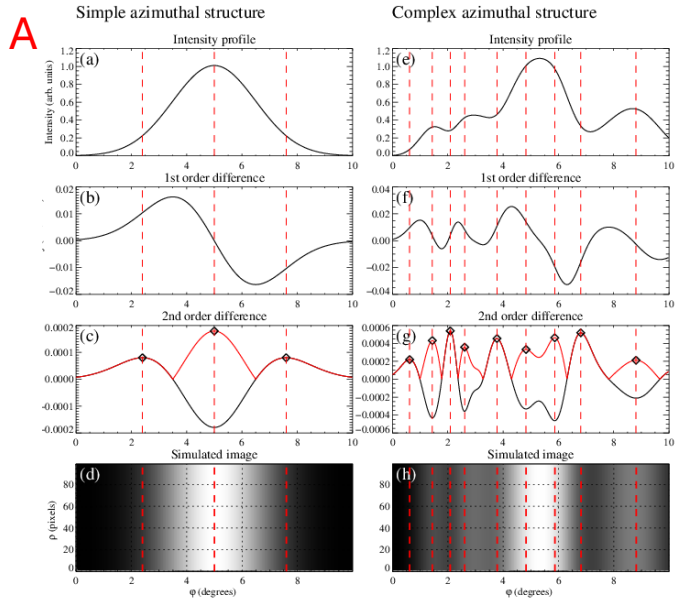


C

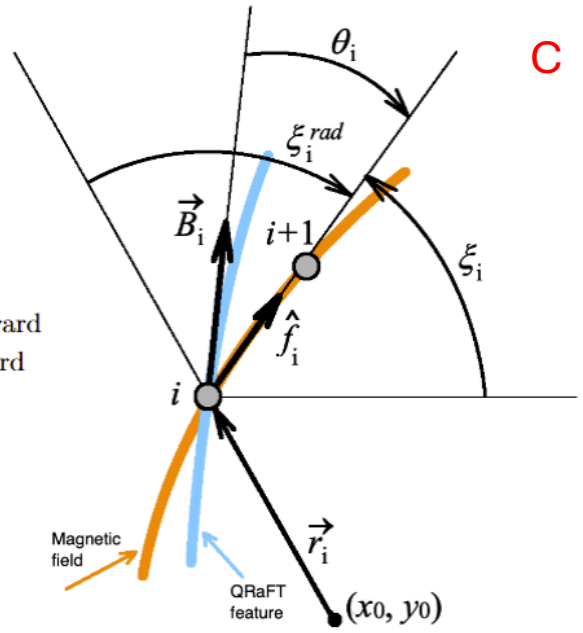

# Performance tests and error analysis MAS/FORWARD + STEREO/COR1

**TSE on Aug-Sep 2017, CR 2194**

MAS model (PSI):
predicted magnetic field lines

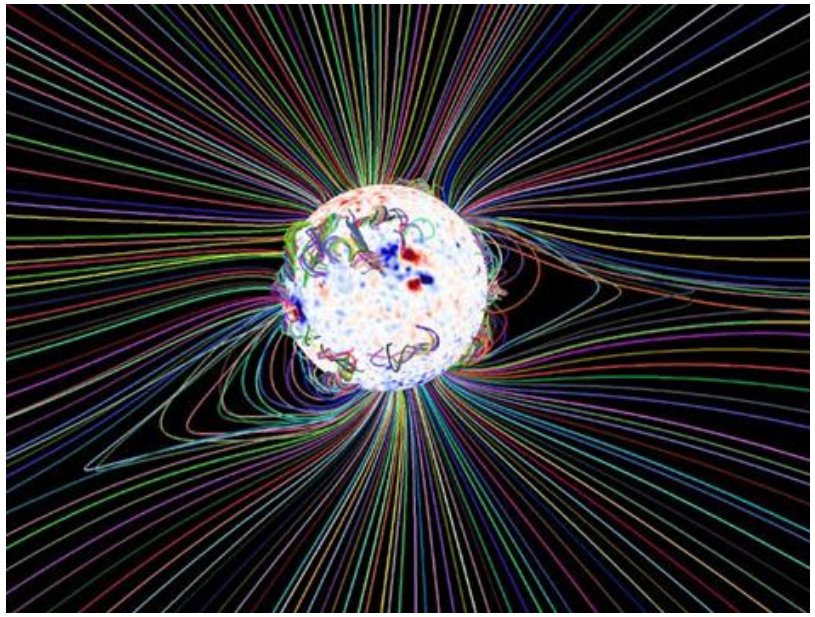

MAS-based synthetic corona:
predicted polarized brightness

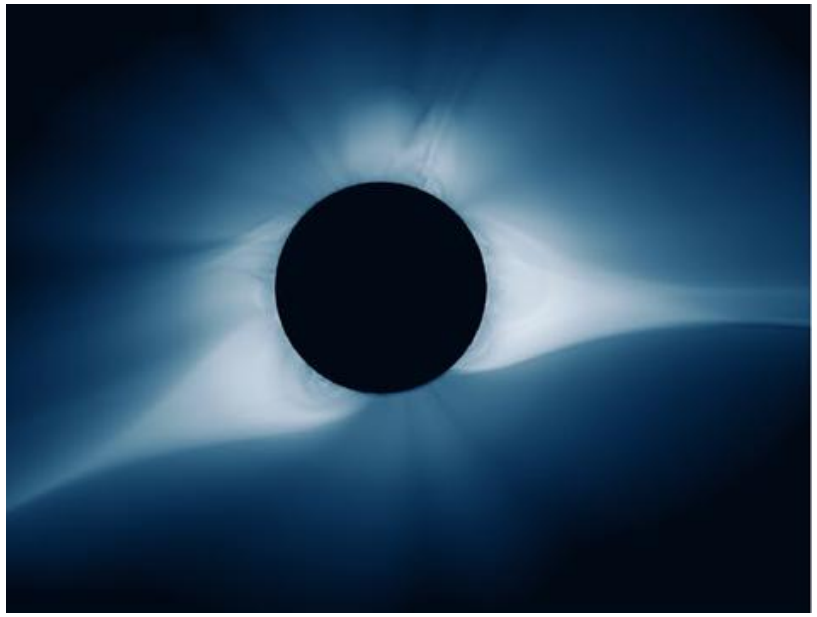

Coaligned coronal observations
by STEREO/SECCHI/COR1

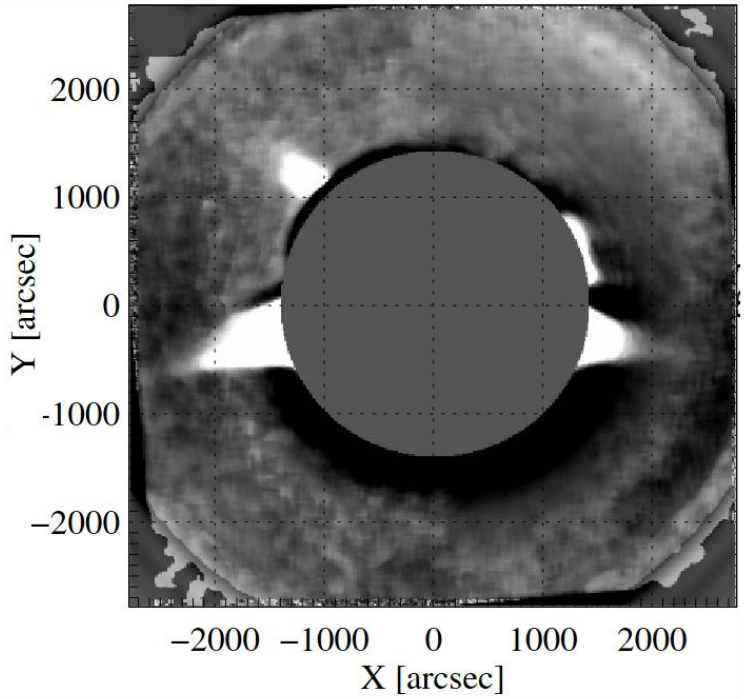


Z. Mikic et al., Predicting the corona for the 21 August 2017 total solar eclipse, Nature Astronomy 2018
S. Gibson et al., FORWARD: A Toolset for Multiwavelength Coronal Magnetometry, Front. Astron. Space Sci 2016.

# QRaFT processing of synthetic and observed corona

## PSI MAS density

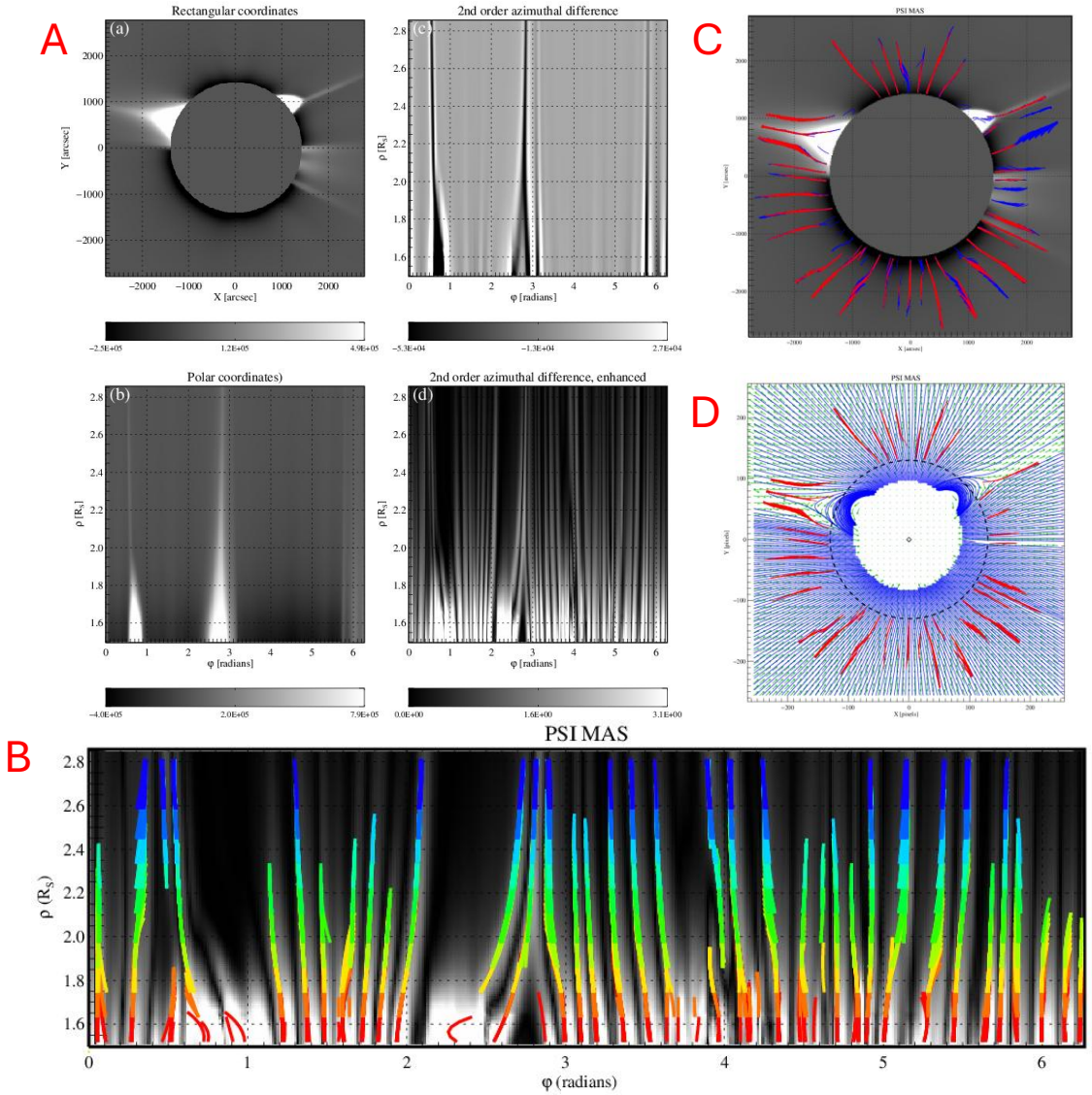


## STEREO COR1 pB

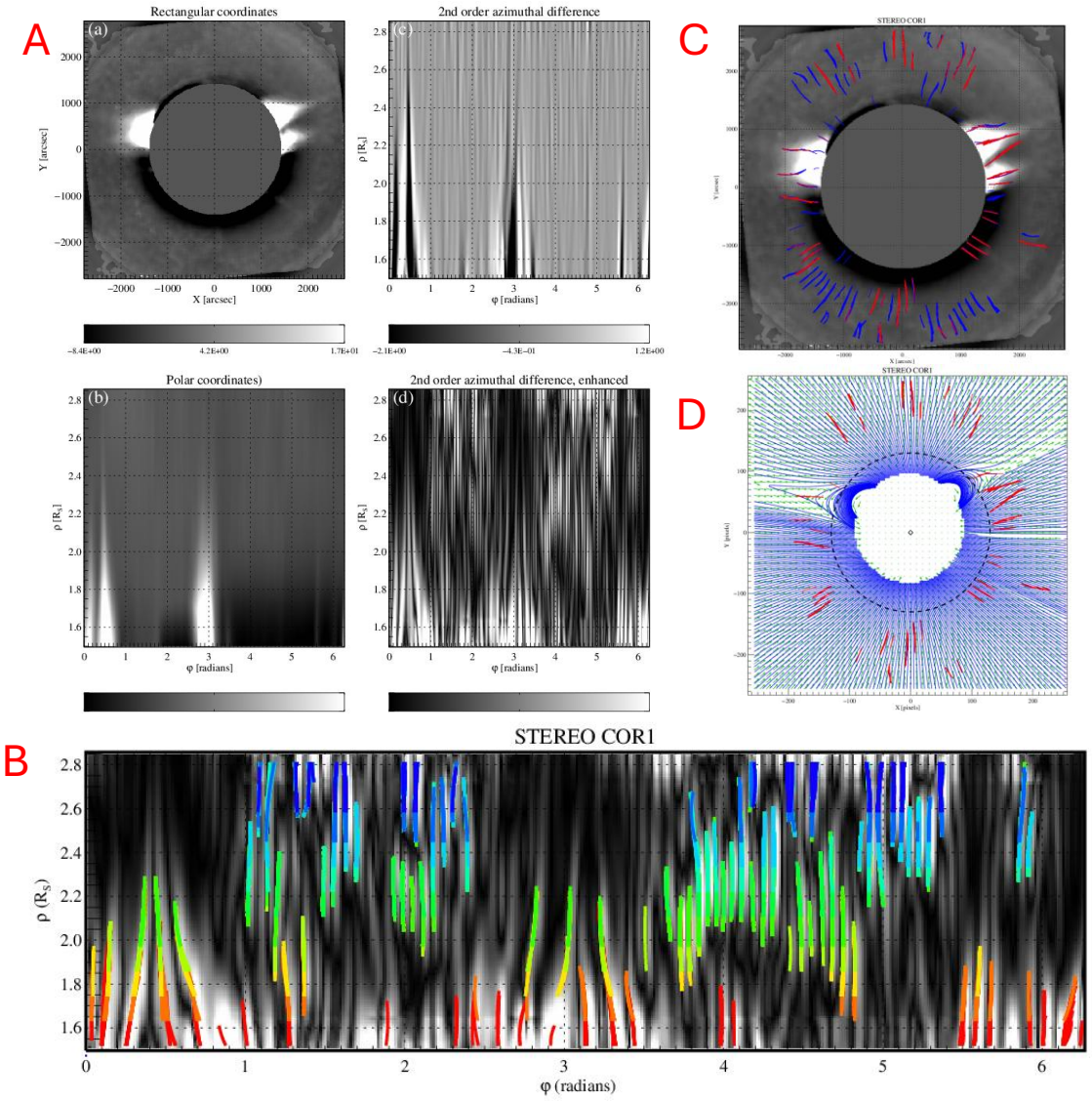

# Feature misalignment errors and their sources

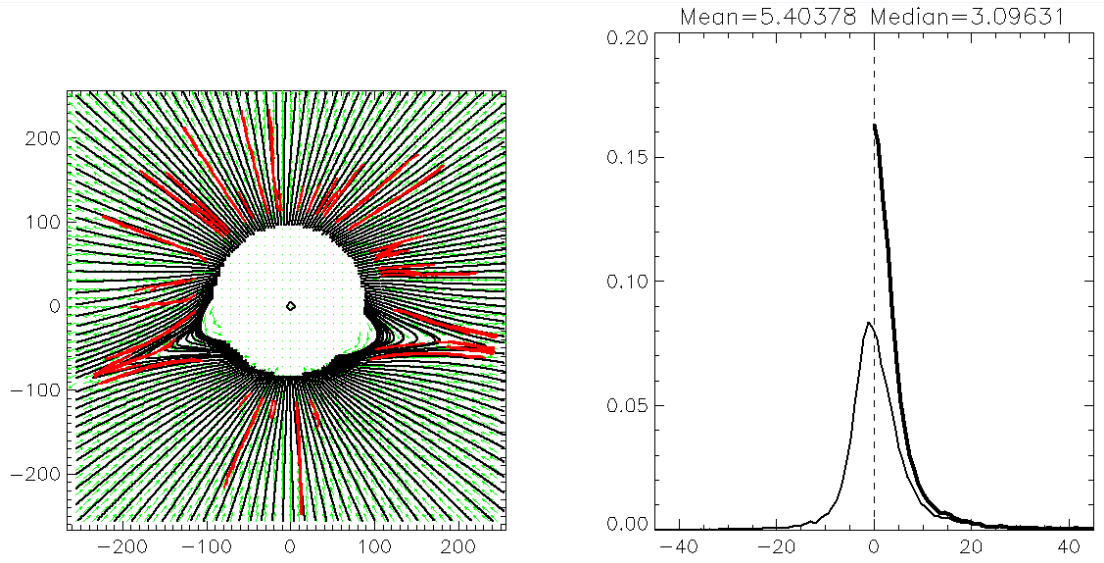


**Main sources of uncertainty**

MAS B vs MAS-based image

1. Local physics
2. LOS projection effects
3. Thomson scattering geometry
4. QRaFT tracing errors
5. FORWARD errors

MAS B vs COR1 image

Items 1-4, plus model discrepancy

| data type | date | mean | median | std | 95% CI | n | kurtosis | skewness |
|---|---|---|---|---|---|---|---|---|
| MAS $n_e$ LOS | 2017-08-25 | 7.408 | 4.477 | 8.949 | 0.184 | 9059 | 8.127 | -0.003 |
| MAS $n_e$ POS | 2017-08-20 | 8.150 | 4.182 | 12.429 | 0.251 | 9444 | 12.444 | -0.342 |
| MAS $n_e$ POS | 2017-08-29 | 8.202 | 5.219 | 10.214 | 0.204 | 9584 | 8.884 | 1.028 |
| FORWARD pB | 2017-08-25 | 8.368 | 4.656 | 9.997 | 0.227 | 7473 | 4.945 | -0.103 |
| MAS $n_e$ LOS | 2017-08-29 | 8.736 | 5.294 | 11.454 | 0.191 | 13878 | 9.642 | -0.157 |
| MAS $n_e$ LOS | 2017-09-03 | 9.062 | 5.802 | 9.724 | 0.236 | 6512 | 3.402 | 0.592 |
| MAS $n_e$ POS | 2017-09-03 | 9.344 | 6.063 | 10.480 | 0.249 | 6793 | 6.902 | -0.722 |
| MAS $n_e$ LOS | 2017-08-20 | 9.724 | 5.234 | 12.902 | 0.265 | 9077 | 6.654 | 0.505 |
| MAS $n_e$ POS | 2017-08-25 | 9.848 | 5.151 | 14.176 | 0.297 | 8739 | 8.983 | 0.404 |
| MAS $n_e$ POS | 2017-09-11 | 10.008 | 7.179 | 11.774 | 0.252 | 8409 | 8.996 | 0.510 |
| FORWARD pB | 2017-08-29 | 10.302 | 5.601 | 14.190 | 0.278 | 9999 | 7.222 | -0.589 |
| FORWARD pB | 2017-08-20 | 10.448 | 5.787 | 13.403 | 0.318 | 6843 | 5.740 | 0.721 |
| FORWARD pB | 2017-09-03 | 10.478 | 6.812 | 11.499 | 0.319 | 5001 | 3.365 | 0.503 |
| COR-1 pB | 2017-08-29 | 11.193 | 7.858 | 12.718 | 0.334 | 5568 | 6.179 | 1.712 |
| MAS $n_e$ LOS | 2017-09-11 | 11.333 | 6.577 | 14.279 | 0.324 | 7481 | 5.293 | -0.657 |
| COR-1 pB | 2017-08-25 | 12.210 | 8.031 | 12.360 | 0.363 | 4455 | 4.446 | 0.117 |
| FORWARD pB | 2017-09-11 | 14.350 | 9.227 | 16.636 | 0.456 | 5113 | 4.082 | -0.461 |
| COR-1 pB | 2017-09-03 | 14.925 | 8.984 | 17.080 | 0.613 | 2981 | 3.855 | 1.692 |
| COR-1 pB | 2017-09-06 | 16.075 | 12.273 | 14.820 | 0.409 | 5047 | 2.141 | -0.328 |
| MAS $n_e$ LOS | 2017-09-06 | 16.309 | 10.018 | 17.747 | 0.334 | 10821 | 3.165 | -0.578 |
| COR-1 pB | 2017-08-20 | 16.615 | 8.021 | 19.529 | 0.542 | 4990 | 2.492 | -0.079 |
| COR-1 pB | 2017-09-11 | 16.633 | 11.681 | 16.153 | 0.454 | 4856 | 1.905 | -1.312 |
| MAS $n_e$ POS | 2017-09-06 | 16.662 | 9.071 | 18.900 | 0.373 | 9864 | 2.231 | 0.063 |
| FORWARD pB | 2017-09-06 | 18.281 | 11.925 | 18.689 | 0.390 | 8836 | 2.548 | -0.671 |

| data type | date | mean | median | std | 95% CI | n | kurtosis | skewness |
|---|---|---|---|---|---|---|---|---|
| MAS $n_e$ POS | combined | 10.479 | 5.996 | 13.855 | 0.118 | 52833 | 7.108 | 0.270 |
| MAS $n_e$ LOS | combined | 10.504 | 6.035 | 13.348 | 0.110 | 56828 | 6.547 | -0.256 |
| FORWARD pB | combined | 12.119 | 6.883 | 14.961 | 0.141 | 43265 | 5.034 | -0.295 |
| COR-1 pB | combined | 14.554 | 9.157 | 15.694 | 0.184 | 27897 | 3.377 | -0.003 |
| random | combined | 45.246 | 45.421 | 25.929 | 0.239 | 45205 | -1.196 | 0.005 |

**C. Rura et al., ApJ 2025 (in preparation)**

# Conclusions

1. The Quasi-Radial Field-line Tracing (QRaFT) image analysis framework has been developed for reconstructing the structure of open-flux coronal regions over a wide range of heliocentric distances.
2. We presented the results of a quantitative testing of QRaFT using MAS global magnetohydrodynamic simulations and the examples of its application to STEREO COR1 pB images.
3. **The estimated error of QRaFT field line tracing of pB coronagraphic images is of the order of 7–12 degrees.**
4. Validation results suggests that QRaFT is capable of reconstructing the geometry of the outermost solar corona and the young solar wind targeted by the upcoming PUNCH mission.
5. QRaFT segmentation of PUNCH data could result in new quantitative metrics for measuring the performance of global heliospheric models and improving space weather forecasts.

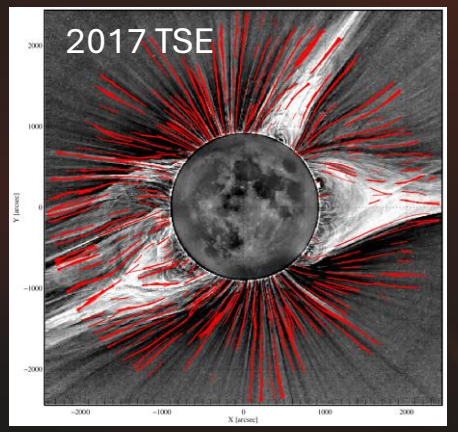


**github.com/uritsky/QRaFT**